Electronic Supplementary Information file for "Electron transport in carbon wires contacted to Ag electrodes: a detailed *first principles* investigation"

Paolo Bonardi,[a] **Simona Achilli,**[a,b] **Gian Franco Tantardini,**[a,b] **and Rocco Martinazzo**[a,b,†]

Electronic structure analysis

Technicalities

We describe here some details of the electronic structure of the carbon atom chains described in the main text, focusing in particular on the changes occurring during adsorption of the molecular species on the Ag surface, *e.g.* the evolution of its electronic energy levels, the build-up of the interactions between the metal and the molecule and the transfer of electrons between the two species. To this end we performed additional calculations on the -C_8H radical species –taken as a representative member of the -C_{2m}- family– and on similar -SC_8SH and -SiC_8SiH species, and followed their electronic structure along an adsorption path. Calculations were performed with a set-up similar to that adopted in the main text, but for a few changes which were necessary in order to correctly describe the systems at large molecule-surface separation, and which are detailed below.

Similarly to the calculations described in the main text, we used periodic, pseudopotential Density Functional Theory (DFT), as implemented in the SIESTA package[1], employing the Perdew-Burke-Ernzerhof (PBE) functional in the generalized gradient approximation (GGA)[2,3] to handle exchange-correlation effects. Core electrons were described by separable, norm-conserving pseudopotentials[4] and a set of atomic orbitals with compact support of double-ζ plus polarization quality was used to expand the wavefunction. Cut-off radii of the atomic orbitals were determined by setting the confinement energy to 0.02 Ry and an energy cutoff of 300 Ry was adopted for the real-space integration of the electron density. A 2×2 supercell was chosen along the Ag(100) surface and Brillouin zone sampling was performed following the Monkhorst-Pack scheme[5] using a 5×5 k-mesh for the self-consistent steps. Geometry optimizations were performed on a 9-layer Ag(100) slab in which the two topmost surface layers were let free to optimize along with the molecular degrees of freedom, and a large vacuum layer was introduced. The tests molecules were placed at several heights z above the surface, *i.e.* at their optimal position at each high-symmetry site and at $\Delta z = 1.0, 2.0, 3.0$ and 5.0 $\AA$ above it*.

Differently from the main text, the calculations described in this document used (i) a cell with an increased height (50 Å), (ii) the self-consistent dipole correction[6] and (iii) an additional top layer of Ag ghost-functions. These improvements were necessary to correctly describe the electrostatic potential above the surface, hence the correct position of the molecular energy levels when the molecule moves along an

[a] *Universitá degli Studi di Milano, Dipartimento di Chimica, via Golgi 19, 20133 Milano, Italy.*
[b] *Consiglio Nazionale delle Ricerche, Istituto di Scienze e Tecnologie Molecolari, Milano, Italy.*
†To whom correspondence should be addressed. E-mail: rocco.martinazzo@unimi.it

∗ The vertical shift was applied to the first C atom only and the structures were then re-optimized exactly as described above, apart from fixing the height of such atom above the surface.

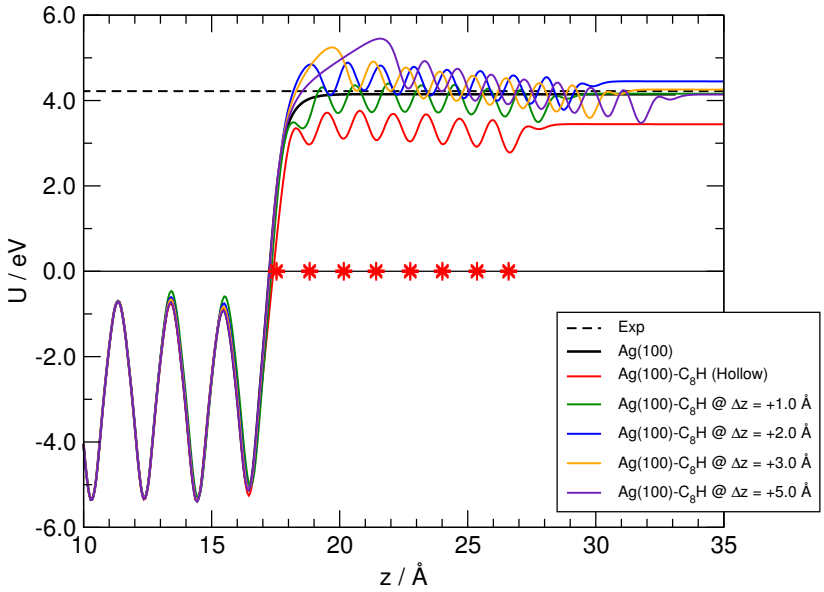

Fig. 1 Averaged electrostatic potential energy along the surface normal for adsorption of a C_8H radical in a hollow site (energy is referenced to the Fermi level). Thick black line is for Ag only, and horizontal line is the experimental value of the Ag(100) work function. Red curve is for C_8H in its optimized geometry above a hollow site of the surface (red stars show schematically the C atom positions in this structure). The remaining curves are for C_8H at shifted positions above the surface, $\Delta z = +1.0, +2.0, +3.0$ and $+5.0$ Å for green, blue, orange and violet.

adsorption path. In particular, only with such improved set-up the surface work function takes a reasonable value of 4.14 eV (in good agreement with the experimental value of[7] 4.22 eV) and this prevents artificial charge transfer to occur at *large* molecule-surface distances. Fig. 1 shows the laterally averaged electrostatic potential energy $U(z) = -|e|\phi(z)$ computed with our set-up for different heights of the molecule above the surface along an hollow adsorption path (values referenced to the Fermi level).

Pure Carbon chains

A summary of the changes in the electronic structure accompanying adsorption at a hollow site is provided by Fig. 2, which compares the Projected Density of States (PDOS) and the Crystal Orbital Hamiltonian Population (COHP) curves, vertically displaced for clarity, from bottom to top for increasing height of the molecule above the surface. PDOS (per atom) are given in the leftmost panel for the top-most Ag atoms closest to the molecule, both for the σ (*i.e.* C(2s,2p$_z$)) orbital of the binding C end and for the π orbitals of the carbon chain, and were computed by applying a 0.05 eV broadening to the Kohn-Sham eigenvalues.

Well above the surface, the molecular energy levels closely resemble those of the isolated radical species and feature four, doubly degenerate π states below the Fermi level describing the occupied π orbitals. With the same token, in the energy range displayed in Fig. 2, only a sharp σ peak appears, $\sim$0.6 eV below the Fermi level, which should represent the 'singly' occupied σ state†. Integration of the spectral densities up to the Fermi level, though, reveals that when the molecule is far from the surface one electron is transferred from the π orbitals to the σ one: the DOS projected on the σ orbitals of the terminal C atom integrates to *three* electrons (one more than expected for a radical with an unpaired electron in a $\sigma(sp)$ state and a σ bond with the neighboring C atom), whereas the projection on the π states of the whole chain integrate to 15 electrons. This suggests that the actual ground-state of the C_8H radical species is of Π symmetry.

† A number of peaks appear at much lower energies ($\lesssim$ -10 eV) representing σ orbitals which spread over the chain.

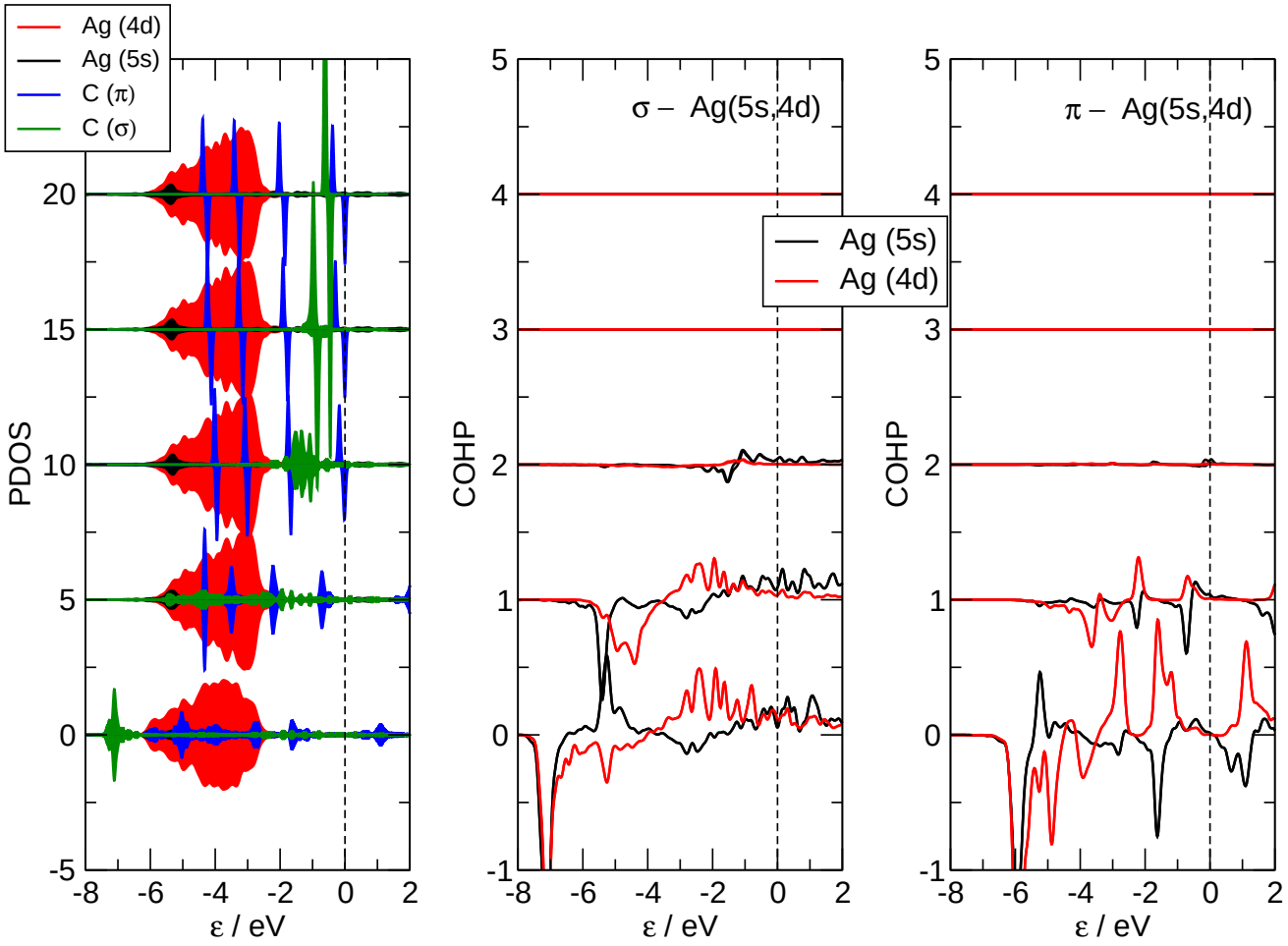

Fig. 2 Evolution of the Ag-C_8H electronic structure along an adsorption path to the stable hollow position. From bottom to top results refer to the optimized structure, and to structures which are shifted upwards by $\Delta z = +1.0, +2.0, +3.0$ and $+5.0$ Å. Left panels: PDOS (per atom) on the surface Ag(4d) and Ag(5s) orbitals (red and black curves, respectively), on the π orbtials of the chain (blue) and on the σ orbital of its unsaturated C end. Results have been vertically shifted for clarity and portrayed for spin majority (upper curves) and spin minority (lower curves) components as usual. Middle panels: COHP curves for the interaction between the σ orbital of the unsaturated C-end of the chain and the 5s and 4d orbitals of the Ag(100) surface (black and red curves, respectively). Right: same as in the middle panel for the π orbitals of the chain. PDOS are per atom in eV^{-1}, and COHP curves are adimensional. See text for details.

When the molecule gets closer to the surface the energy level broadens and downshift in energy because hybridization with Ag orbitals of the surface atoms occurs. Such hybridization is particularly effective for the σ state, as expected, but is substantial also for the π states too. The latter, of course, are those involved in charge transport at low energy, hence π-hybridization, though less dramatic than its σ counterpart, has a major effect in the transport properties of the junction, as shown at length in the article. The changes in the electronic structure of the surface closely parallel the above spectral transformations. In particular, the Ag(5s) peak (the projection of the s band on the surface atoms) widens and finally disappears when the metal-molecule bond is formed, but also the Ag(4d) spectral density broadens and downshift in energy, thereby signalling a favorable interaction with the molecular levels.

To gain insights into the hybridization process, we analyzed four different kinds of COHP curves[‡]: C(σ)/Ag(5s), C(σ)/Ag(4d), C(π)/Ag(5s) and C(π)/Ag(4d), where C is the carbon atom involved in the bond formation process. As is well known, COHP/COOP are valuable tools to investigate interactions in periodic structures at a level similar to overlap population analysis in molecular orbital theory; negative (positive) COHP values indicate bonding (antibonding) interactions (and the converse for COOP), hence COHP/COOP unfold information which could be hardly extracted from PDOS only[8,9]. The middle and right panels of Fig. 2 show, respectively, that hybridization is strongly bonding for $E \lesssim$-4 eV for both the σ and the π orbitals of the C atom at the chain end, and moderately antibonding at higher energies (due mainly to the antibonding hybridization with Ag($4d$) orbitals established by both σ and π states).

Fig. 3 shows a comparison of the electronic structure of AgC_8H when adsorption occurs at hollow, bridge and top sites (from bottom to top). The results reported on the left panels clearly indicate an increasing interaction (*i.e.* broadening and shifting of the molecular resonances) in the order top ¡ bridge ¡ hollow, similarly to what is shown in the main article for the molecular resonances of -C_n- bridging two metal electrodes. The middle and the right panels make evident that while hybridization of the σ orbitals in similar in the three cases, hybridization of the π states is of increasing magnitude along the same sequence. Noteworthy is the behavior of the C(π)-Ag(5s) hybridization which is at maximum for adsorption at the hollow site and vanishes for adsorption on top of a Ag atom (for symmetry reasons).

We further analyzed charge transfer at the level of simple Mulliken analysis (this is equivalent to integrate the DOS projected on the atoms), considering -C_n- chains bridging two Ag(100) electrodes, since this situation directly relates to the electronic transport problem. Fig. 4 shows the σ and π Mulliken charges for $n = 12$, when binding occurs at the hollow, bridge and top sites. Comparison with the Mulliken charges computed at the same level of theory for the gas-phase $HC_{12}H$ molecule shows that charge transfer only involves the C-ends of the chain. In particular, electrons are transferred from the metal to the σ states of the contact atoms (0.25-0.30 $|e|$) and *back-donated* by the π states ($\sim$0.2 $|e|$).

Tunneling

Fig. 5 show the results of the electronic structure analysis for the "tunneling geometry" considered in the main text. Specifically, we considered the shortest molecular bridge -C_2- at its stable hollow adsorption geometry and compared the interactions between opposing metal atoms at the electrode surfaces. Analysis of the DOS projected on the Ag(5s,4d) states (left panel) already shows that in the presence of the C_2 "spacer" the d signal broadens a bit and shifts downward in energy, as a consequence of the bonding interaction with the molecular levels. Less evident, but more relevant for transport, is the change in the DOS projected on the Ag(5s) orbitals; binding of C_2 withdraws spectral weight from the Fermi level and is

‡ The same conclusions follow from the COOP curves (not shown).

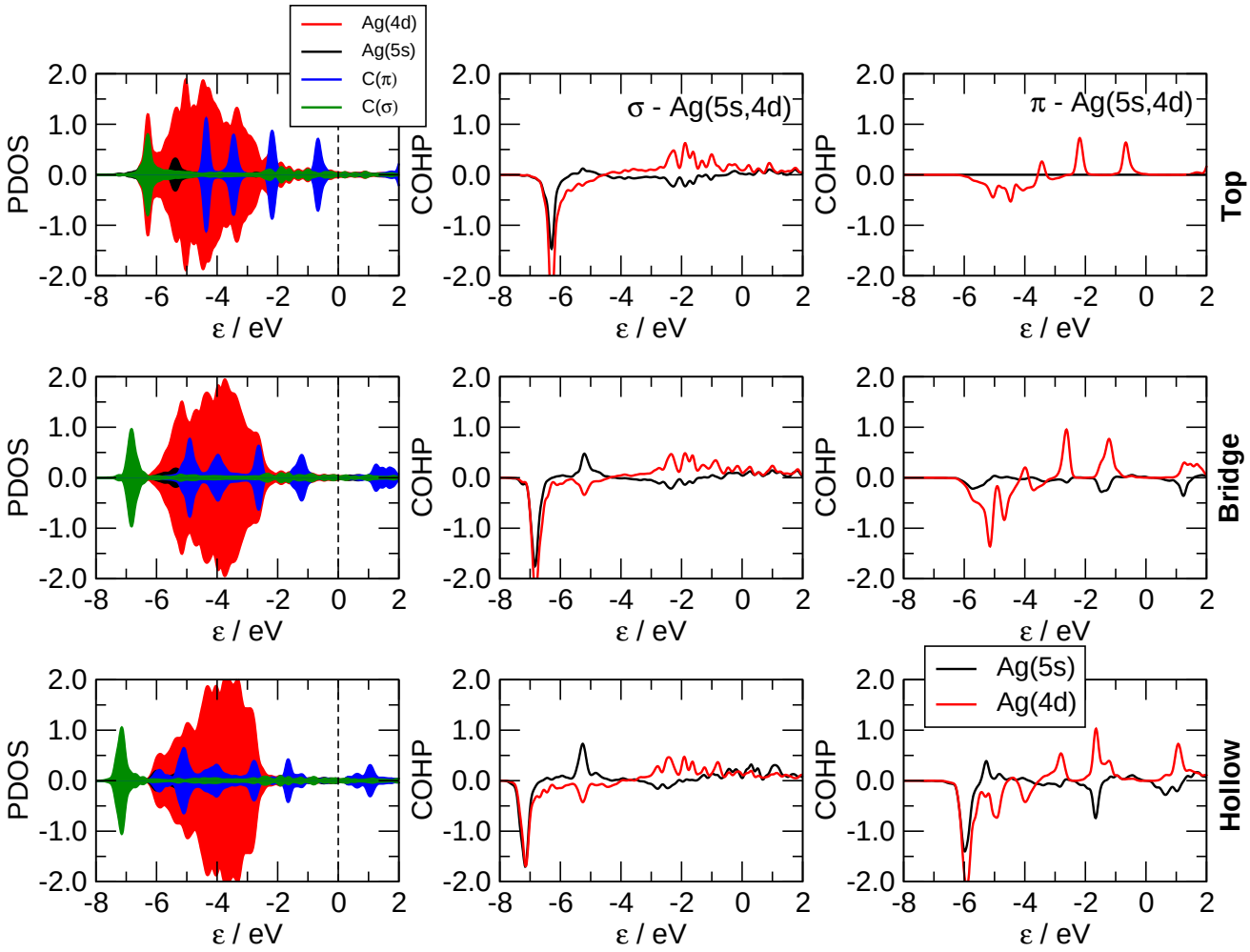

Fig. 3 Same results as in Fig. 2 for C_8H adsorbed in hollow, bridge and top sites, at their corresponding optimized geometries (from bottom to top).

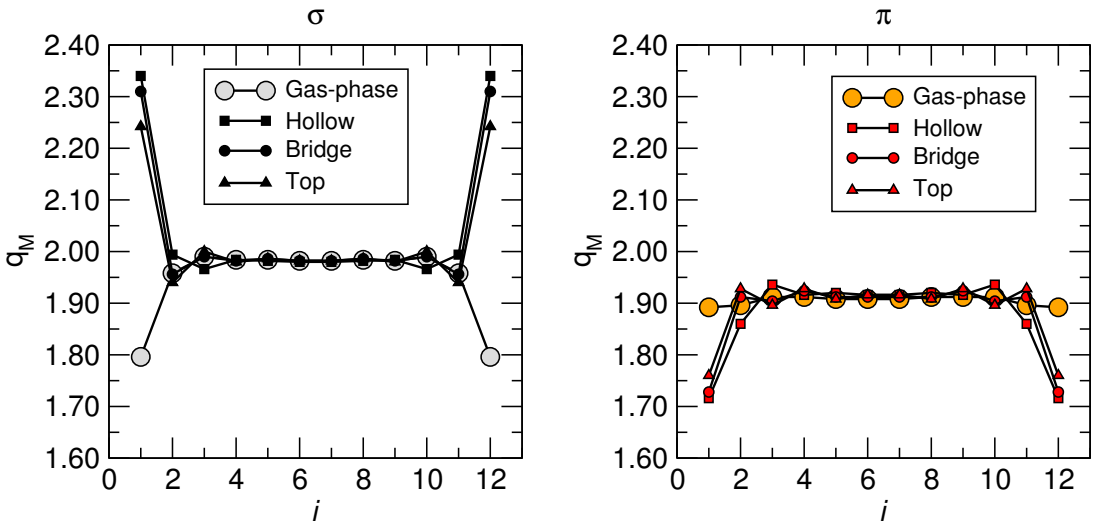

Fig. 4 Mulliken population analysis of a -C_{12}- molecular bridge between hollow (squares), bridge (circles) and top (sites) of the Ag(100) electrodes surface (j labels the carbon atoms along the chain). Left and right panel for the σ and π contributions as obtained upon summing over valence C atom orbitals of appropriate symmetry. Also shown for comparison the same analysis for the gas-phase $HC_{12}H$ molecule.

the likely source of the (small) reduction of the conductance in the presence of molecule discussed in the main text.

Anchoring species

Fig. 6 highlights the main effects that the capping species have on the electronic structure of the contacted molecules. Results are shown for -SC_8SH and -SiC_8SiH at their optimized geometries on the high-symmetry adsorption sites and are compared with those obtained for the uncapped -C_8H species considered above. As can be seen from the figure, the DOSs feature additional π peaks which show that π-conjugation is effectively increased with the anchoring groups under consideration. The main difference between S and Si lies in the number of π electrons added to system, which is nominally *four* for each sulphur atom and *two* for each Si atom; hence, two(one) more occupied π levels appear for S(Si). The case of -SC_8SH requires closer inspection, since Fig. 6 shows that when the molecule adsorbs either in a top or in a bridge position a π peak appears right at the Fermi level[§]. Integration of the PDOS reveals that the σ states of the Sulphur atom actually host *three* electrons, *i.e.* one more than expected for a thiole-like atom Ag-$\underline{\bar{S}}$-C-... This is not due to the hybridization being different from sp, because the molecule remains linear in these structures and the $\sigma - \pi$ orbitals are well defined. Rather, this is due to a charge transfer from the π to the σ states, which makes S to behave as Ag :$\underline{\dot{S}}$-C-.. and leaves a hole in the π system. In the molecular-bridge configuration, one hole is contributed from each S atom, and the middle peak becomes exactly centered at the Fermi level, with two electrons out of a maximum of four allowed.

Fig. 7 shows the bonding/antibonding contributions of the π states centered on the X atom. Here X is the first Sulphur atom in -SC_8SH, the first Silicon atom in -SiC_8SiH and the first carbon atom in -C_8H. COHP curves are shown for the interaction with the Ag(5s) and Ag(4d) orbitals (black and red curves, respectively), and for the interactions with the C(π) orbitals of the neighboring C atom (green).

§ Similar results hold for -SiC_8SiH at a bridge site, but the energetics here is much less favorable that the very existence of such configuration is doubtful (binding is ∼3.7 eV less stable than at the hollow site).

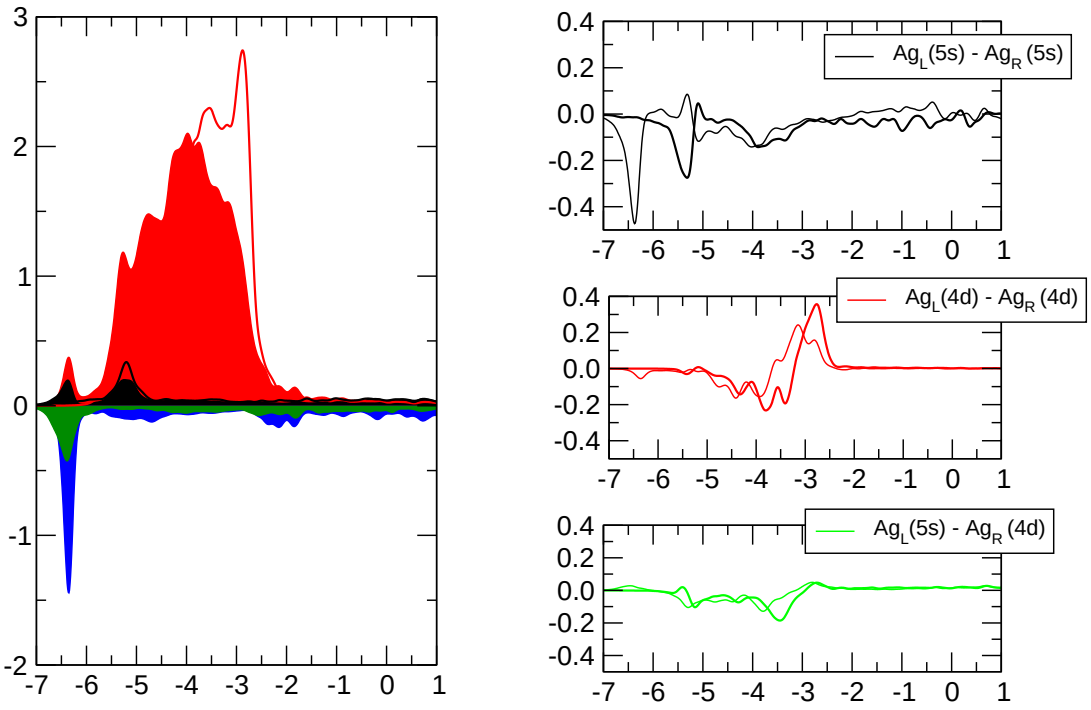

Fig. 5 PDOS (left panel) and COHP (right panels) for the "tunneling geometry" described in the main text, with (thin lines) and without (thick lines) a C_2 spacer between the electrodes. For clarity, in the left panel, every shaded PDOSs refers to the presence of the spacer, and projection on the C atoms are given with negative values (blue and green for π and σ contributions, similarly to Fig.s 2 and 3).

As is evident from Fig. 7 interaction with Ag(5s,4d) orbitals of the surface atoms is sizable only for adsorption at the hollow site. Similarly to the -C_8H case discussed above, X(π)-Ag(5s) interactions disappear in the top position, but now also the X(π)-Ag(4d) are generally reduced for top and bridge adsorption. On the other hand, X(π)-C(π) interactions are in any case strong, and this justifies the picture of a chain which is 'extended' when the anchoring species are S or Si. Notice further that for S, the two highest π peaks are antibonding, in accordance with the arguments given above which would place the Fermi level *above* the middle of the spectrum. In other words, since S(π) states are more than half-filled the Fermi level is shifted upwards, in an energy region where states have antibonding character.

Convergence tests

As mentioned in the main article, we also performed all-electron, linear-response, TD-DFT calculations of the optical properties of gas-phase HC_nH molecules, using different functionals in the adiabatic approximation. To this end we used the Gaussian09 quantum chemistry code[10], with the 6-31++G** basis set and some semilocal (PBE) and hybrid (B3LYP) functionals, both in their original formulation and in their long-range-corrected form[11,12]. The basis-set was chosen after carefully checking its performance in such optical calculations, as shown in Fig. 8 for the $C^1\Sigma_u^+ \leftarrow X^1\Sigma_g^+$ transition in HC_nH (n even, $n = 4-20$). In such figure, the lowest-energy dipole allowed transition in the series was computed with the CAM-B3LYP functional using two different variants of Gaussian basis-sets: the split-valence 6-31G and the correlation consistent sequence cc-pV*m*Z ($m = 2-4$) of Dunning *et al.*[13], either with (right panel) or without (left panel) addition of diffuse functions. Calculations refer to the same set of geometries –which were obtained

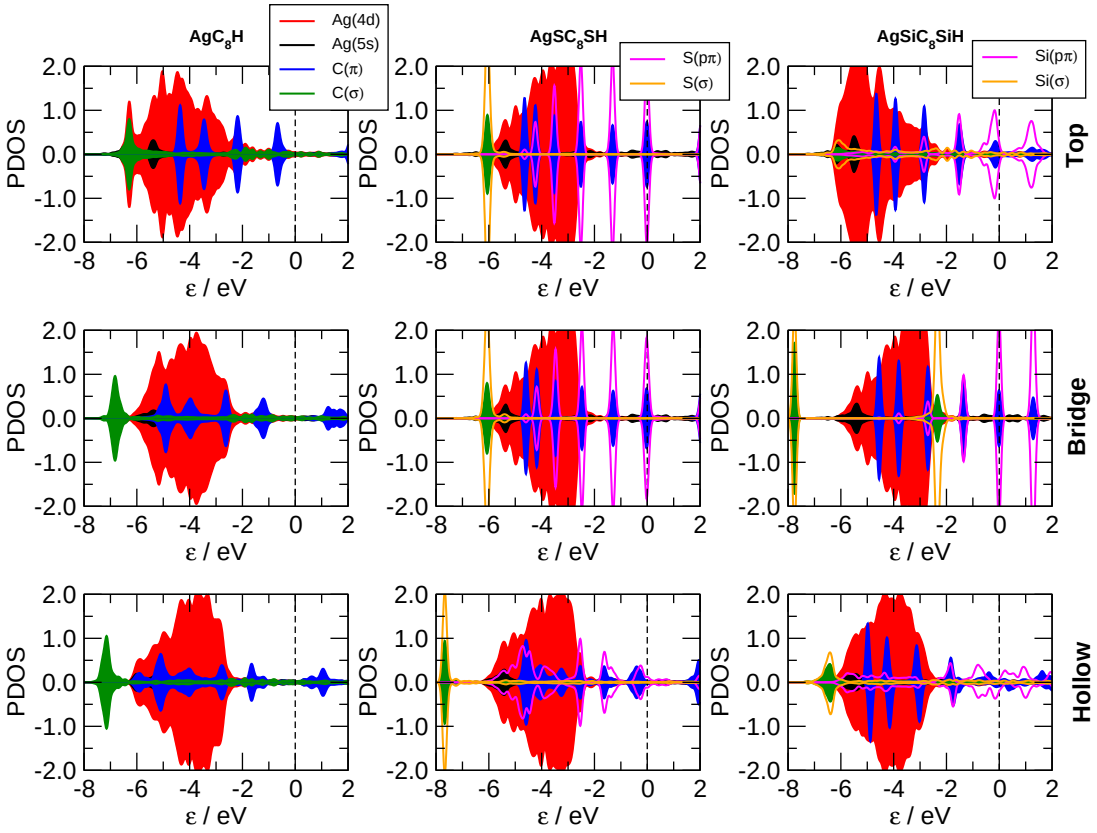

Fig. 6 Density of states of AgC_8H (left column), $AgSC_8SH$ (middle) and $AgSiC_8SiH$ (right) projected on the surface Ag atom(s) closest to the molecule, on the carbon atom chains and on the capping atom bound to the metal. PDOS results are per atom, with red and black curves for the Ag(4d) and Ag(5s) contributions, green (orange) for the contribution of σ orbitals of the C (X) atom closest to the surface (X=S,Si), blue for the π orbitals of the chain and magenta for the $p\pi$ orbitals of X. The different rows represent results obtained for different adsorption sites, hollow, top and bridge, respectively, from bottom to top.

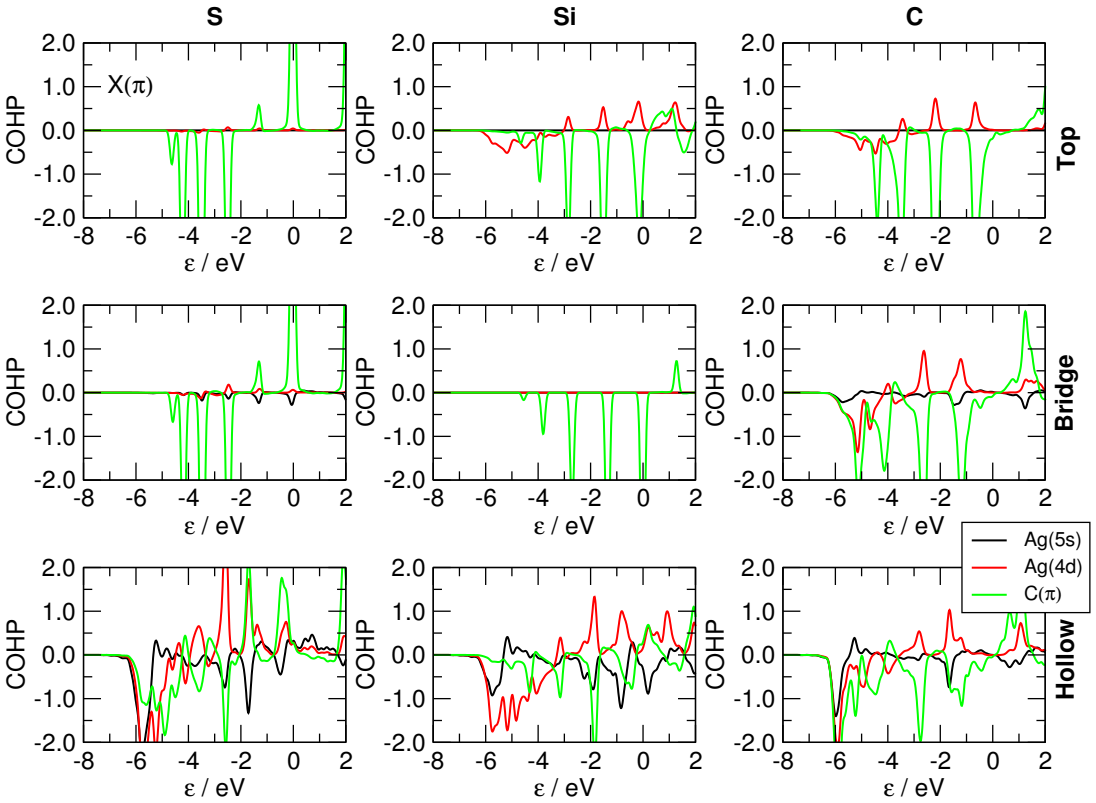

Fig. 7 COHP curves for the interaction of the π orbitals of the contact atom X (X=S,Si,C) with Ag(5s), Ag(4d) orbitals of the surface and the C(π) of the neighboring C atom (black, red and green curves), as computed for $AgSC_8SH$ (left column), $AgSiC_8SiH$ (middle) and AgC_8H (right). The different rows correspond to the different adsorption sites as indicated.

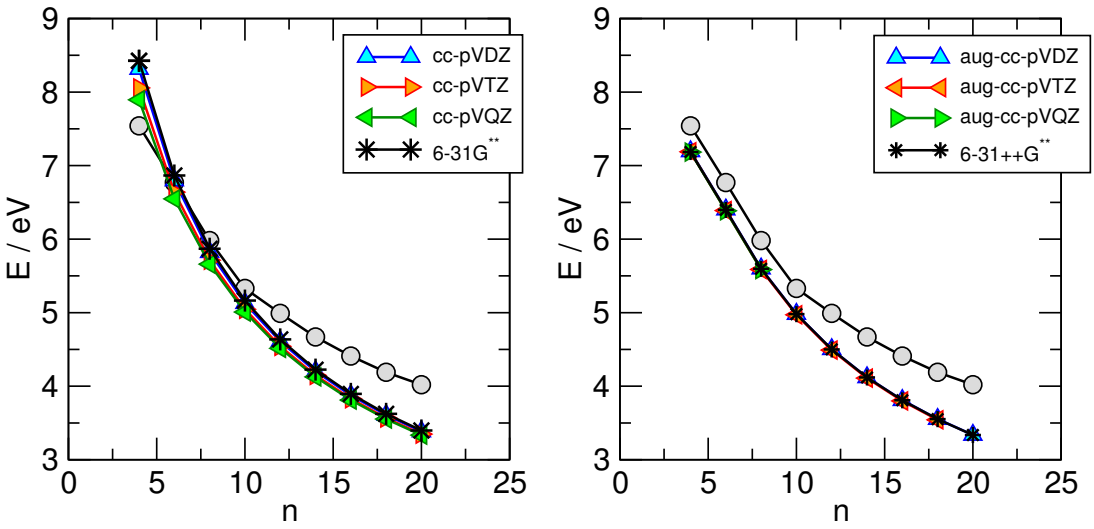

Fig. 8 Basis-set convergence tests performed on the lowest dipole-allowed optical transition in gas-phase HC_nH molecules, as computed at the TD-DFT level using the CAM-B3LYP functional in the adiabatic approximation, and employing a set of reference geometries optimized at the B3LYP/aug-cc-pVDZ level. Results are for Dunning *et al.* (cc-pVnZ, $n = 2, 3, 4$) and Pople 6-31G basis sets, with and without diffuse functions (right and left panel, respectively). Open circles represent experimental data [14].

by geometry optimization at the B3LYP/aug-cc-pVDZ level– and results are compared to experimental values¶. As can be seen from Fig. 8, results here obtained with the modest-size 6-31G set compare favorably with those obtained at the much more expensive cc-pVmZ level, which in turn are rather well converged with respect to the 'correlation level'. Importantly, though, the addition of diffuse functions largely improves the trend of the transition energy *vs.* n (see in particular the change in the slope which appears in the experimental data at around $n = 10$), even though some results ($n = 6, 8, 10$) get worse. This was clearly a fortunate event in the results shown in the left panel, namely a combination of a slightly wrong geometry with a slightly wrong transition energy. The effect of the diffuse function is important for small n only, nevertheless is the key for obtaining very good results over the whole sequence, when the same basis set is used for both geometry optimization and optical calculations (at the CAM-B3LYP level).

References

1 J. M. Soler, E. Artacho, G. J. D., A. García, J. Junquera, P. Ordejón, and D. Sánchez-Portal, J. Phys.: Condens. Matter **14**, 2745 (2002).
2 J. P. Perdew, K. Burke, and M. Ernzerhof, Phys. Rev. Lett. **77**, 3865 (1996).
3 J. P. Perdew, K. Burke, and M. Ernzerhof, Phys. Rev. Lett. **78**, 1396 (1997).
4 N. Troullier and J. L. Martins, Phys. Rev. B **43**, 1993 (1991).
5 H. J. Monkhorst and J. D. Pack, Phys. Rev. B **13**, 5188 (1976).
6 L. Bengtsson, Phys. Rev. B **59**, 12301 (1999).
7 M. Chelvayohan and C. H. B. Mee, Journal of Physics C: Solid State Physics **15**, 2305 (1982).
8 R. Hoffmann, Angewandte Chemie International Edition in English **26**, 846 (1987).
9 R. Dronskowski and P. E. Bloechl, The Journal of Physical Chemistry **97**, 8617 (1993).

¶ As mentioned in the article, production runs used the 6-31++G** set, and optimized geometries were obtained for each functional considered. Hence, the results shown in the article for CAM-B3LYP refer to geometries optimized at the CAM-B3LYP level and are much better than those reported here.

10 M. J. Frisch, G. W. Trucks, H. B. Schlegel, G. E. Scuseria, M. A. Robb, J. R. Cheeseman, V. G. Zakrzewski, J. A. M. Jr., R. E. Stratmann, J. C. Burant, et al., *Gaussian09, Revision A.02* (Gaussian Inc., Pittsburgh PA, 2009).
11 H. Iikura, T. Tsuneda, T. Yanai, and K. Hirao, J. Chem. Phys. **115**, 3540 (2001).
12 T. Yanai, D. P. Tew, and N. C. Handy, Chem. Phys. Lett. **393**, 51 (2004).
13 J. Thom H. Dunning, J. Chem. Phys. **90**, 1007 (1989).
14 R. Nagarajan and J. P. Maier, Int. Rev. Phys. Chem. **29**, 521 (2010).